

Article

Reconstruction of Composite Stiffness Matrix with Array-Guided Wave-Based Genetic Algorithm

Menglong Liu ^{1,*}, Yaohui Zhang ¹, Lun Li ¹, Gongfa Chen ² and Fangsen Cui ^{3,*}¹ School of Mechanical Engineering and Automation, Harbin Institute of Technology, Shenzhen 518055, China² School of Civil and Transportation Engineering, Guangdong University of Technology, Guangzhou 510006, China³ Institute of High Performance Computing, Agency for Science, Technology and Research, Singapore 138632, Singapore

* Correspondence: liumenglong@hit.edu.cn (M.L.); cui fs@ihpc.a-star.edu.sg (F.C.)

Abstract: Accurate measurement of the material parameters of composite in a nondestructive manner is of great significance for evaluating mechanical performance. This study proposes to use a genetic algorithm (GA) to reconstruct the stiffness matrix of carbon fiber reinforced polymer (CFRP) with array-guided wave (GW)-based GA. By comparing the numerically calculated GW dispersion curves with the experimental wave number-frequency contour calculated with a two-dimensional Fourier transform (2D-FFT), the matching coefficient is directly obtained as the objective function of the GA, avoiding the overhead of sorting out the respective GW modes. Then the measured stiffness matrix with tensile testing and the longitudinal wave in the unidirectional CFRP is compared with the reconstructed parameters from unidirectional, cross-ply, and quasi-isotropic CFRPs with the GA. For the four independent parameters, excluding C_{12} , an average value of 11.62% for the maximum deviation is achieved among the CFRPs with three stacking sequences, and an average deviation of 11.03% in unidirectional CFRPs is achieved for the parameters measured with different methods. A further correction of fiber orientation results in a relative deviation of only 2.72% for the elastic modulus along the tensile direction, and an expansion of the GW frequency range for the GA narrows down the relative deviation of C_{12} to 3.9%. The proposed GW-based GA opens up a way of in situ and nondestructive measurement for the composite stiffness matrix.

Keywords: guided wave; carbon-fiber-reinforced polymer; genetic algorithm; stiffness matrix

Citation: Liu, M.; Zhang, Y.; Li, L.; Chen, G.; Cui, F. Reconstruction of Composite Stiffness Matrix with Array-Guided Wave-Based Genetic Algorithm. *Materials* **2022**, *15*, 8715. <https://doi.org/10.3390/ma15248715>

Academic Editor: Ricardo J. C. Carbas

Received: 29 October 2022

Accepted: 3 December 2022

Published: 7 December 2022

Publisher's Note: MDPI stays neutral with regard to jurisdictional claims in published maps and institutional affiliations.



Copyright: © 2022 by the authors. Licensee MDPI, Basel, Switzerland. This article is an open access article distributed under the terms and conditions of the Creative Commons Attribution (CC BY) license (<https://creativecommons.org/licenses/by/4.0/>).

1. Introduction

With the recent improvement in manufacturing technology, a variety of materials are woven, wound, laminated, etc., to form new composite materials, such as fiber-reinforced polymer laminates, Kevlar, ceramic matrix composite materials, etc. [1–3]. Compared with traditional metal materials, these new composite materials have significantly different structural forms and material properties, which will directly affect the mechanical properties and intended functions of the material. Moreover, in the processing, manufacturing, and service period of the materials, the molding process conditions (temperature, pressure, time, casting, forging, etc.), external loads, material aging, environmental temperature, humidity changes, etc. will inevitably lead to changes in the mechanical parameters of the material, or cause a change in the size, shape, and performance of the structure. For example, the elastic modulus value of fiber-reinforced composites can be used to characterize (1) whether the material meets the manufacturing requirements and (2) the real-time performance during service [4]. To withstand high temperatures, the surface layer of ceramic matrix composites will erode during service [5]. The wall thickness of the pipeline structure is often used as an important evaluation criterion for the severity of pipeline corrosion [6]. If the changes in the above-mentioned structural thickness and material parameters cannot

be evaluated timely and accurately, they will seriously affect the normal service or functioning of the structure, thereby causing damage to the structure. Therefore, for these complex materials and structures, it is necessary to accurately characterize the structural and material parameters [7].

There are four main existing experimental techniques for measuring material parameters (mainly elastic modulus or stiffness matrix), including techniques based on quasi-static loading, sub-resonance, resonance, and wave propagation. The quasi-static-loading-based technology uses an external loading device to load a specimen with a specific size, and a single test can only obtain a single material parameter [8,9]. The sub-resonance-based technique calculates the elastic modulus and internal friction according to the acquired load-displacement response relationship when the excitation frequency of the structure is less than the first-order resonance frequency. This method is suitable for materials under laboratory conditions. Representative equipment includes commercial dynamic mechanical analyzers and Kê pendulum clocks [10]. Resonance technology is currently the most widely used method for testing material parameters in the laboratory. Typical methods include the free-free beam method [11] and the pulse excitation method [12], both of which are based on the bending or torsional resonance frequency of a rectangular bar specimen to measure the material's elastic modulus. However, the accuracy of this method is strongly dependent on the support location and support method. The resonance ultrasonic spectroscopy method [13], which is also based on resonance technology, obtains multiple resonance frequencies through a single measurement and then adopts the inverse algorithm to match the resonance frequencies measured by numerical calculation and experiment and can measure all 21 independent elastic constants with a sample of specific dimensions under laboratory conditions.

From the review of the four main existing experimental techniques for measuring material parameters, it is concluded that these techniques mainly focus on the characterization of material parameters in the laboratory with samples of specific sizes. Thus, there still exists a gap in in situ and nondestructive measurements. Instead, stress waves exhibit the characterization potential of material and structural parameters, which control the characteristics of wave propagation. Several bulk wave-based techniques were developed to obtain the material parameters [14]. For composites, there exist multiple independent elastic modulus parameters whose parameter identification was made possible with bulk wave data propagating in multiple directions [15–17]. In addition, multiple material parameters jointly determine the wave velocity. It is necessary to calculate the error between the multiple measurement data and the theoretical value, establish the objective function (OF), and use the GA [18], Newton-Raphson method [19], simplex method [18], and other inverse problem algorithms to obtain the optimal solution for multiple parameters. The bulk-wave-based technique is usually used with thick materials, as a thin sample will cause a large measurement error in wave velocity.

Different from the propagation of ultrasonic bulk waves, Guided waves (GWs) propagate along the guided direction of the waveguide and feature a propagation velocity that varies with the frequency and the coexistence of multiple modes [20,21]. Thus, the propagation characteristics are jointly governed by the geometrical dimensions of the waveguide structure and the material's mechanical parameters. To obtain the GW dispersion curve, the commonly used signal excitation and acquisition methods include the piezoelectric wafer [22], non-contact laser [23,24], ultrasonic piezoelectric array probe [25], etc. Compared with the contact-based signal acquisition method that the probe may influence the signal quality, and the non-contact method offers more accurate data.

In the research on constructing a matching index between the theoretical and experimental GW characteristics, the multi-mode and dispersion characteristics of GWs bring rich information but also pose challenges. Foiret et al. [25] used a linear array to collect the GW signal on a cortical bone, constructed the OF using the difference between the theoretical calculation and the experimental results, and obtained the thickness and wave speed of the bone. The GWs can only be extracted manually by trained researchers, making the method

difficult to implement practically. Eremin et al. [26] manually picked the fundamental A_0 and S_0 modes, whose wavelengths were input into a GA for parameter reconstruction of unidirectional and cross-ply carbon fiber reinforced polymer (CFRP) laminate. Further, an unsupervised learning method based on the mode separation of a GW was proposed to characterize the material parameters of multiple isotropic materials [27]. Similarly, Okumura et al. [28] adopted a diagonal loading technique to quickly extract a GW curve in an isotropic material. Lu et al. [29] proposed a hybrid particle swarm-based-simulated annealing optimization technique to obtain the elastic properties of the isotropic plate structure, but multiple GW curves need to be extracted first, which is difficult to apply in complex structures. Zhao et al. [23] first converted the experimentally measured group velocities of a GW fundamental mode in the 360-degree circumferential directions into phase velocities, manually selected a specific mode, and then used the error between the theoretical and experimental phase velocities to construct the OF. Hu et al. [30] further developed the hybrid Lasso regression to improve the experimental signal-to-noise ratio of a GW along one single direction for the reconstruction of the material stiffness matrix.

In the above research, the dispersion curve of the GW needs to be extracted from the experimentally acquired data either manually or with some signal processing methods, which may be quite complex when higher-order GW modes are involved in a wide frequency range. In order to overcome the dependence on the extraction of GW modes, Bochud et al. [31] proposed a positive and negative value method by substituting the experimental contour with a wavenumber-frequency domain into the theoretical GW equation for single-layer weakly anisotropic materials, which can automatically construct an OF, but the method is limited to single-layer materials and does not demonstrate the ability to generalize to complex multilayer structures with strong anisotropy such as CFRP.

In summary, the existing structural and material parameter reconstruction methods based on ultrasonic bulk waves are mainly used for large-thickness materials. Meanwhile, the existing techniques based on a GW, because the multi-mode and dispersion characteristics make it difficult to effectively identify each mode, rely heavily on the manual classification of GW modes from experimental results to establish a matching target that minimizes experimental and computational errors. In addition, the information from different GW propagation directions has yet to be fully used for a more robust parameter reconstruction of a CFRP with strong anisotropy.

Addressing the above problems, this study proposes an automatic reconstruction of the CFRP material stiffness matrix with the GW-based GA. The stiffness matrix for comparison in this study is obtained based on data from the tensile loading and longitudinal wave. In addition, the proposed method does not rely on any manual selection of specific GW modes and adopts a GA to realize the reconstruction of the stiffness matrix of lamina based on a GW in CFRP laminates with unidirectional (UD), cross-ply (CP), and quasi-isotropic (QI) stacking sequences.

The rest of the paper is organized as follows. Section 2 details the experimental setups and methods of static tensile loading and longitudinal wave testing to obtain one set of the stiffness matrix and the GW testing to obtain multiple sets of the stiffness matrix of CFRPs with different stacking sequences. Section 3 analyzes the sensitivity of material parameters on GW characteristics, the deviation of reconstructed parameters, and the further refinement of several key parameters. Concluding remarks are provided in Section 4.

2. Materials and Methods

The static tensile loading and longitudinal wave testing were performed first to obtain the stiffness matrix of UD; then, the GW testing was performed to acquire the array of GW signals, which were input into the GA for the reconstruction of the stiffness matrix.

2.1. Experimental Setup

2.1.1. Static Tensile Loading

For the unidirectional CFRP sample with the fiber along the x axis, y - z plane can be treated approximately as a plane of isotropy, and thus the stress (σ) to strain (ϵ) relation is given as

$$\begin{bmatrix} \sigma_1 \\ \sigma_2 \\ \sigma_3 \\ \sigma_4 \\ \sigma_5 \\ \sigma_6 \end{bmatrix} = \begin{bmatrix} C_{11} & C_{12} & C_{12} & 0 & 0 & 0 \\ C_{12} & C_{22}^\dagger & C_{23} & 0 & 0 & 0 \\ C_{12} & C_{23} & C_{22}^\dagger & 0 & 0 & 0 \\ 0 & 0 & 0 & C_{44} & 0 & 0 \\ 0 & 0 & 0 & 0 & C_{55} & 0 \\ 0 & 0 & 0 & 0 & 0 & C_{55} \end{bmatrix} \begin{bmatrix} \epsilon_1 \\ \epsilon_2 \\ \epsilon_3 \\ \epsilon_4 \\ \epsilon_5 \\ \epsilon_6 \end{bmatrix}, \quad (1)$$

where σ_i denotes the normal or shear stress, ϵ_i denotes the normal or engineering shear strain, C_{ij} denotes the parameters of stiffness matrix, in which C_{22}^\dagger is not independent and can be given by the following linear combination of two other elements

$$C_{22}^\dagger = C_{23} + 2C_{44}, \quad (2)$$

leaving the number of independent elements in the stiffness matrix of Equation (1) to be five. These five independent elements can also be converted into five numbers consisting of elastic moduli E_1 , E_3 , and G_{13} , and Poisson's ratios ν_{13} and ν_{23} .

Static tensile loading of the UD sample, as displayed in Figure 1, was performed to measure four parameters, including E_1 , E_3 , ν_{13} , and G_{13} . The parameters of CFRP samples, load, and sensor for tensile loading are listed in Table 1. Every third sample of the nine samples (250 mm \times 25 mm) was cut along the x direction, 45° to the x direction, and along the z direction, respectively. A universal testing system (ZwickRoell® 20 kN Allround tabletop, Ulm, Germany) was used for tensile loading. A 350 Ω strain gauge (BE350-3AA-P100, ZEMIC Group, Xi'an, China) bonded normal to the loading direction was connected to the dynamic strain amplifier (KYOWA® DPM-911B, Tokyo, Japan), whose output voltage was acquired with an oscilloscope (Keysight® Infiniium MXR058A, Colorado Springs, CO, USA). Another 350 Ω strain gauge bonded along the loading direction was connected directly to the digital multimeter (Keithley® DMM7510, Tektronix, Inc., Beaverton, OR, USA), whose acquired value of electrical resistance was proportional to the measured strain value.

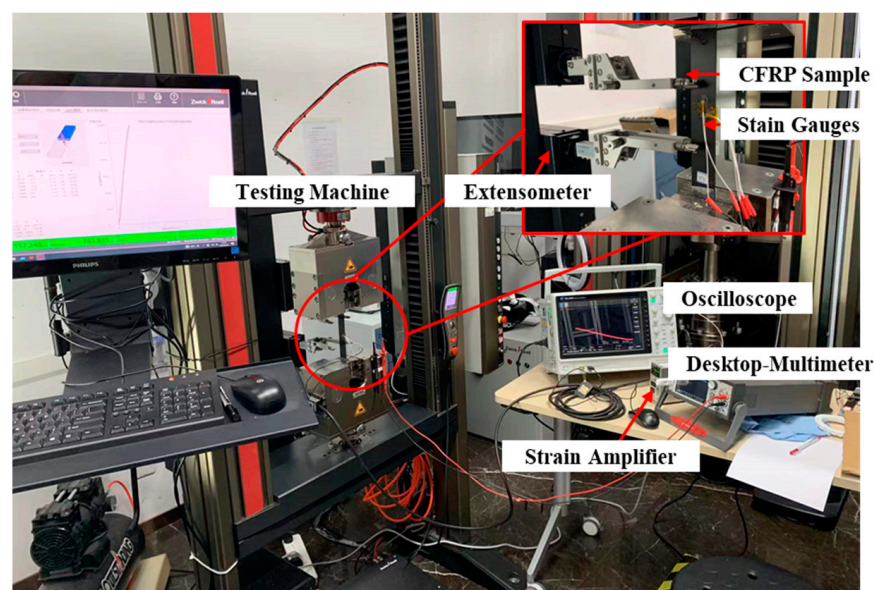


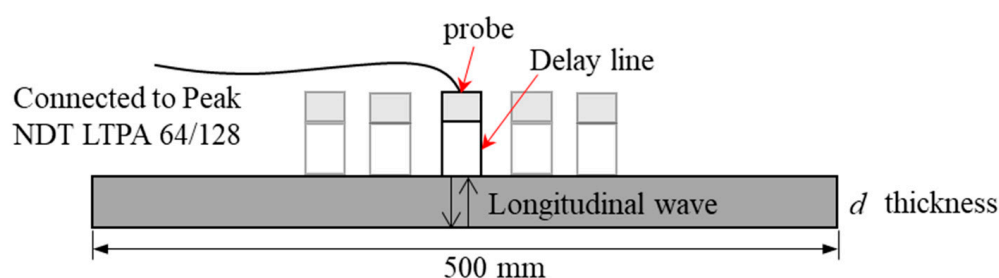
Figure 1. Experimental setup of static loading.

Table 1. Parameters of CFRP samples, load, and sensor for tensile loading.

Cutting Direction	Size (mm)	Maximum Load (kN)	Resistance of Strain Gauge (Ω)
0°	250 × 25	2 for 0°	350
45°		1.5 for 45°	
90°		1 for 90°	

2.1.2. Longitudinal Wave Testing

To measure the last parameter v_{23} in the UD sample, longitudinal wave testing was performed, as displayed in Figure 2. A delay line piezoelectric probe with a central frequency of 15 MHz was excited via the conventional channel of the multi-channel pulse exciter/receiver (Peak NDT® LTPA 64/128, Derby, UK), acting as both pulse transmitter and receiver unit. Five random locations were selected to calculate the average arrival time of echo signals. A sampling rate of 100 MHz was adopted for signal acquisition.

**Figure 2.** Experimental setup of longitudinal wave testing.

2.1.3. Guided Wave Testing

Laminates (500 mm × 500 mm) with three stacking sequences were fabricated, which are listed in Table 2, together with the average thickness and density.

Table 2. CFRP sample specification.

No.	Stacking Sequence	Thickness (mm)	Density (kg/m ³)
1	[0] ₁₆	2.05	1507.2
2	[0/90] _{4s}	2.17	1490.5
3	[0/90/0/90/45/−45/45/−45] _s	2.27	1480.1

The GW testing was performed as shown in Figure 3, with key parameters listed in Table 3. A three-cycle Hanning window modulated sinusoidal signal at a center frequency of 400 kHz was amplified to 800 V_{pp} via the gated high-power radio frequency pulse amplifier (Ritec® GA-2500A, Warwick, RI, USA), and output to the piezoelectric wafer (Φ 8 mm, 0.48 mm thick) bonded on the surface of the CFRP sample. The wave signal was acquired with the laser vibrometer (Tecnar® LUS discovery, Saint-Bruno, QC, Canada) after a sample averaging 512 times. The plate was fixed to a stepper motor with a movement increment of 1 mm and a total movement distance of 128 mm. In this way, out-of-plane displacements at 128 points were acquired along both the horizontal (x) and vertical (z) directions.

Table 3. Parameters of GW testing.

CFRP Size (mm)	Piezoelectric Wafer	Excitation Central Frequency (kHz)	Array Spacing (mm)	Point Number
500 × 500	Φ 8, 0.48 thick	400	1	128

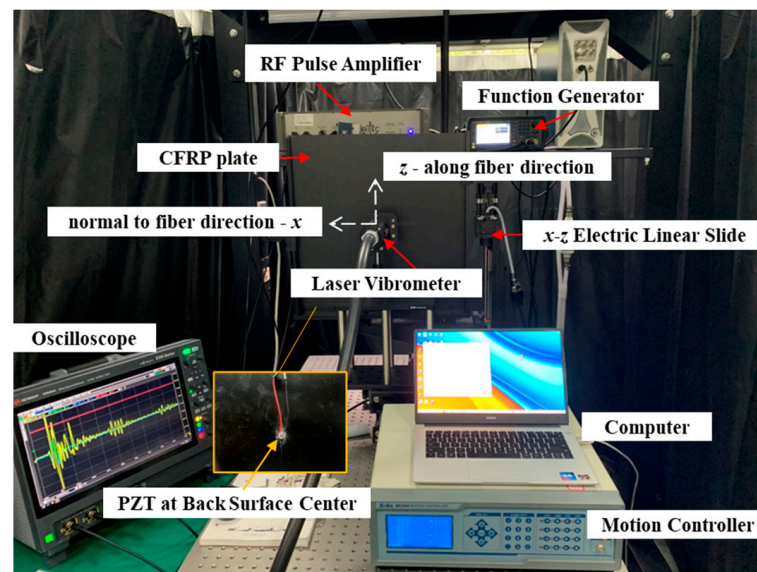


Figure 3. Experimental setup of GW testing.

2.2. Methods

2.2.1. Derivation of Material Parameters with Tensile Loading

The derivation of the four parameters based on the static tensile loading of UD is as follows:

- (1) Young's modulus along the fiber direction E_1 ;

$$E_1 = \frac{\sigma_{1-1}}{\varepsilon_{1-1}} = \frac{N_1}{A\varepsilon_{1-1}} \quad (3)$$

where σ_{1-1} , ε_{1-1} , and N_1 denote the longitudinal stress, strain, and loading force with the sample cut along the fiber direction, and A is the cross-sectional area.

- (2) Young's modulus normal to the fiber direction E_3 ;

$$E_3 = \frac{\sigma_{3-3}}{\varepsilon_{3-3}} = \frac{N_3}{A\varepsilon_{3-3}} \quad (4)$$

where σ_{3-3} , ε_{3-3} , and N_3 denote the longitudinal stress, strain, and loading force with the sample cut normal to the fiber direction.

- (3) Poisson's ratio ν_{13} ;

$$\nu_{13} = \frac{\varepsilon_{3-1}}{\varepsilon_{1-1}} \quad (5)$$

where ε_{3-1} and ε_{1-1} denote the transverse and longitudinal strains with loading to the sample along the fiber direction.

- (4) Shear modulus G_{13} ; The Young's modulus E_{45° of the sample cut along 45° to the x direction is related to E_1 , E_3 , ν_{13} , and G_{13} as follows:

$$\frac{1}{E_{45^\circ}} = \frac{1}{4} \left(\frac{1}{E_1} + \frac{1}{E_3} + \frac{1}{G_{13}} - \frac{2\nu_{13}}{E_1} \right) \quad (6)$$

thus G_{13} can be calculated provided the known E_1 , E_3 , ν_{13} , and E_{45° .

2.2.2. Derivation of Material Parameter with Longitudinal Wave

1. Poisson's ratio ν_{23} ; The longitudinal wave testing was performed to measure the last parameter ν_{23} , as illustrated in Figure 2. The average velocity of the longitudinal wave is measured experimentally as

$$v_L = \frac{1}{5} \sum_{i=1}^5 \frac{2d_i}{\Delta t_i} \quad (7)$$

where d is the measured thickness and Δt is the time of flight of the pulse-echo. The measurement is performed at five random locations with $i = 1, 2, 3, 4, 5$. The velocity is related to E_3 and ν_{23} as

$$v_L^2 \rho = C_{22} = \frac{1 - \nu_{12}\nu_{21}}{N} E_2 \quad (8)$$

where

$$N = 1 - 2\nu_{12}\nu_{21} - \nu_{23}\nu_{32} - 2\nu_{21}\nu_{32}\nu_{13} \quad (9)$$

via which ν_{23} can be derived.

2.2.3. Derivation of Material Parameters with GW-Based GA

The flowchart of parameter reconstruction with GW-based GA is illustrated in Figure 4. Based on the desired image resolution in the frequency domain, the 128 time-domain signals along both directions acquired with the laser vibrometer were zero-filled to desired lengths before the operation of 2D-FFT. Then the original wave number at $[1000/128 \times 2\pi: 1000/128 \times 2\pi: 2000\pi]$ was linearly interpolated to the desired resolution. Finally, the experimental spectrogram M_{exp} of frequency-wave number domain at the range of 0–500 kHz and 0–2000 rad/m with the desired resolution was generated. On the other hand, the theoretical dispersion curve of GW was initially calculated with a semi-analytical finite element (SAFE) developed by the authors [32], in which the wave number was swept from 0 to 2000 rad/m at the desired resolution to obtain the exact solution of the frequency with the input material parameters. Then the exact solution was rounded to the nearest frequency value at the desired resolution in the frequency domain to obtain the theoretically calculated image M_{cal} .

In order to reconstruct $C_{11}, C_{12}, C_{22}, C_{23}$, and C_{66} simultaneously, both the signals along the 0° (x) and 90° direction (z) were used in the OF described as

$$F(C_{11}, C_{12}, C_{22}, C_{23}, C_{66}) = M_{\text{cal}}^x M_{\text{exp}}^x + M_{\text{cal}}^z M_{\text{exp}}^z \quad (10)$$

For the UD for which some parameters can be decoupled with the GW along the 0° (x) and 90° direction (z), which is analyzed in Section 3.1, the OF is described as

$$\begin{cases} F(C_{22}, C_{23}) = M_{\text{cal}}^z M_{\text{exp}}^z \\ F(C_{11}, C_{12}, C_{66}) = M_{\text{cal}}^x M_{\text{exp}}^x \end{cases} \quad (11)$$

Figure 5 shows the flowchart of GA for the reconstruction of the stiffness matrix to seek the optimum parameter with the maximum value of OF. A computer with a CPU of Intel(R) Core(TM) i7-9700 CPU@3.00GHz and RAM of 32 GB (Intel Corporation, Santa Clara, CA, USA) was used. MATLAB was adopted to fulfill the calculation of both the GW dispersion curve and GA. The algorithm started randomly generating an initial population of 64. The upper and lower bounds for each parameter were set as 150% and 50%, respectively, of the parameter derived from the static tensile loading and longitudinal wave testing. Every initial parameter increment was set as 0.1 GPa. A uniform crossover with a probability of 0.9 and mutation operations with a probability of 0.5 were then performed. Individual fitness was evaluated by the OF defined in Equations (10) and (11). The algorithm was considered converged when the first 16 values of each parameter with the largest OF remained unchanged.

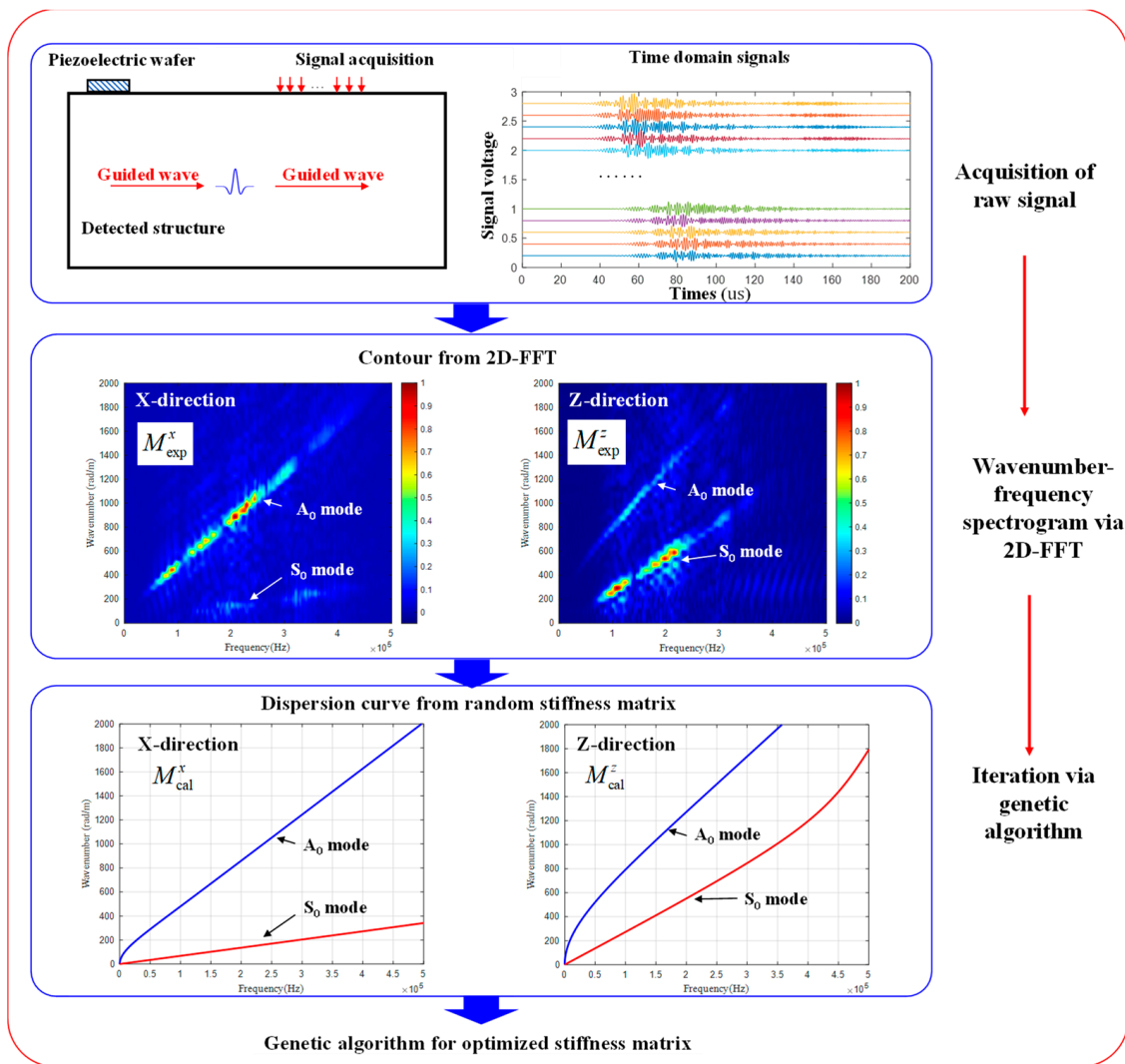


Figure 4. Flowchart of parameter reconstruction based on GA.

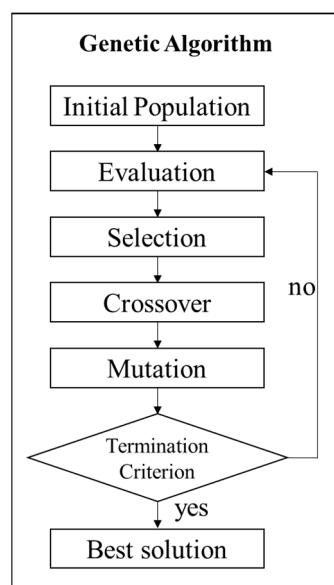


Figure 5. Flowchart of GA for inverse reconstruction of stiffness matrix.

3. Results

According to the five calculated material parameters based on the static tensile loading and longitudinal wave testing, the sensitivity of each parameter on the GW dispersion curve is analyzed, followed by the reconstruction of the material parameter with a GW-based GA.

3.1. Sensitivity Analysis of Parameter on GW Dispersion Curve

According to the results from the static tensile loading and longitudinal wave testing, all five parameters are listed in Table 4, together with the calculated stiffness matrix.

Table 4. Derived stiffness matrix of UD with tensile loading and longitudinal wave.

E_1	E_3	ν_{13}	G_{13}	ν_{23}
99.55 GPa	9.305 GPa	0.3231	4.009 GPa	0.4389
C_{11}	C_{12}	C_{22}	C_{23}	C_{66}
103.1 GPa	5.549 GPa	11.82 GPa	5.352 GPa	4.009 GPa

Taking the UD for investigation, each parameter was changed by 50% while keeping other parameters unchanged, whose corresponding GW dispersion curves are displayed in Figure 6. It is concluded that

- (1) C_{11} mainly influenced S_0 along the fiber direction while independent from the GW normal to the fiber direction.
- (2) C_{12} slightly influenced the GW along the fiber direction while independent from that normal to the fiber direction.
- (3) C_{22} was almost independent of the GW along the fiber direction while largely influencing the GW normal to the fiber direction.
- (4) C_{23} slightly influenced the GW along the fiber direction while largely influencing the GW normal to the fiber direction.
- (5) C_{66} largely influenced the GW along the fiber direction while independent from the GW normal to the fiber direction.

Thus, while using the GW for the reconstruction of the stiffness matrix of UD, C_{12} might exhibit a large error, as a GW along both directions was hardly sensitive to its change. In addition, considering that only C_{22} and C_{23} determined the GW normal to the fiber direction, the five independent parameters were decoupled into two groups. The 1st group included C_{22} and C_{23} , whose values were reconstructed with a GW normal to the fiber direction. Then, the obtained C_{22} and C_{23} were input into the GA as known parameters to reconstruct the value of the 2nd group of parameters including C_{11} , C_{12} , and C_{66} , with a GW along the fiber direction.

Taking the CP and QI for further investigation, the corresponding GW dispersion curves are displayed in Figures 7 and 8, respectively. It was concluded that C_{12} was still insensitive to GW along both directions, which made it hard to be correctly identified. Except for that, other parameters showed the potential of being correctly reconstructed, as the change of parameters all influenced the dispersion curve of the GW in both directions. Thus, all five independent parameters were simultaneously reconstructed with a GW along both directions.

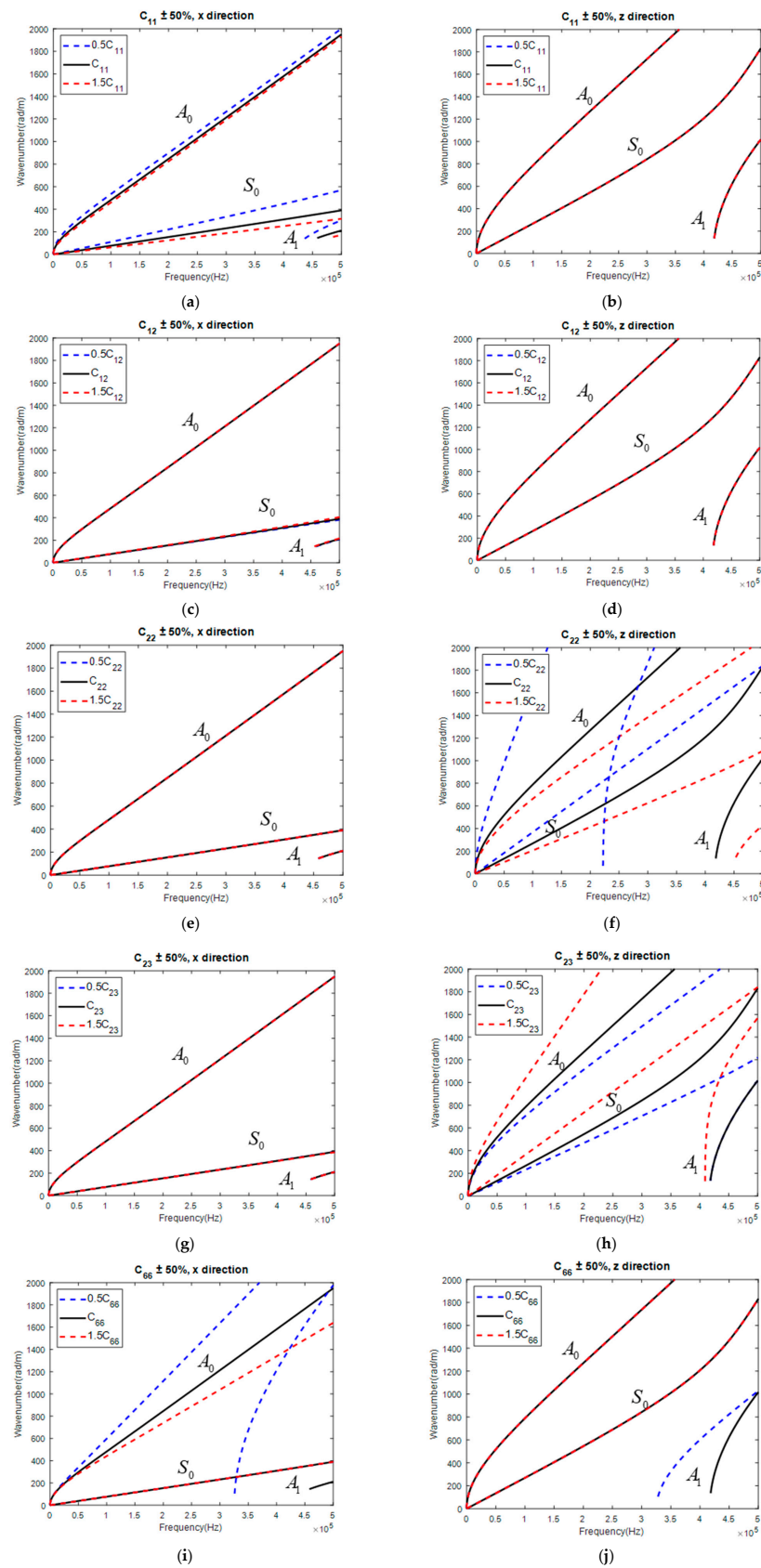


Figure 6. Influence of parameter on GW dispersion curve in UD: C_{11} on GW along (a) x and (b) z direction; C_{12} on GW along (c) x , and (d) z direction; C_{22} on GW along (e) x and (f) z direction; C_{23} on GW along (g) x and (h) z direction; C_{66} on GW along (i) x and (j) z direction.

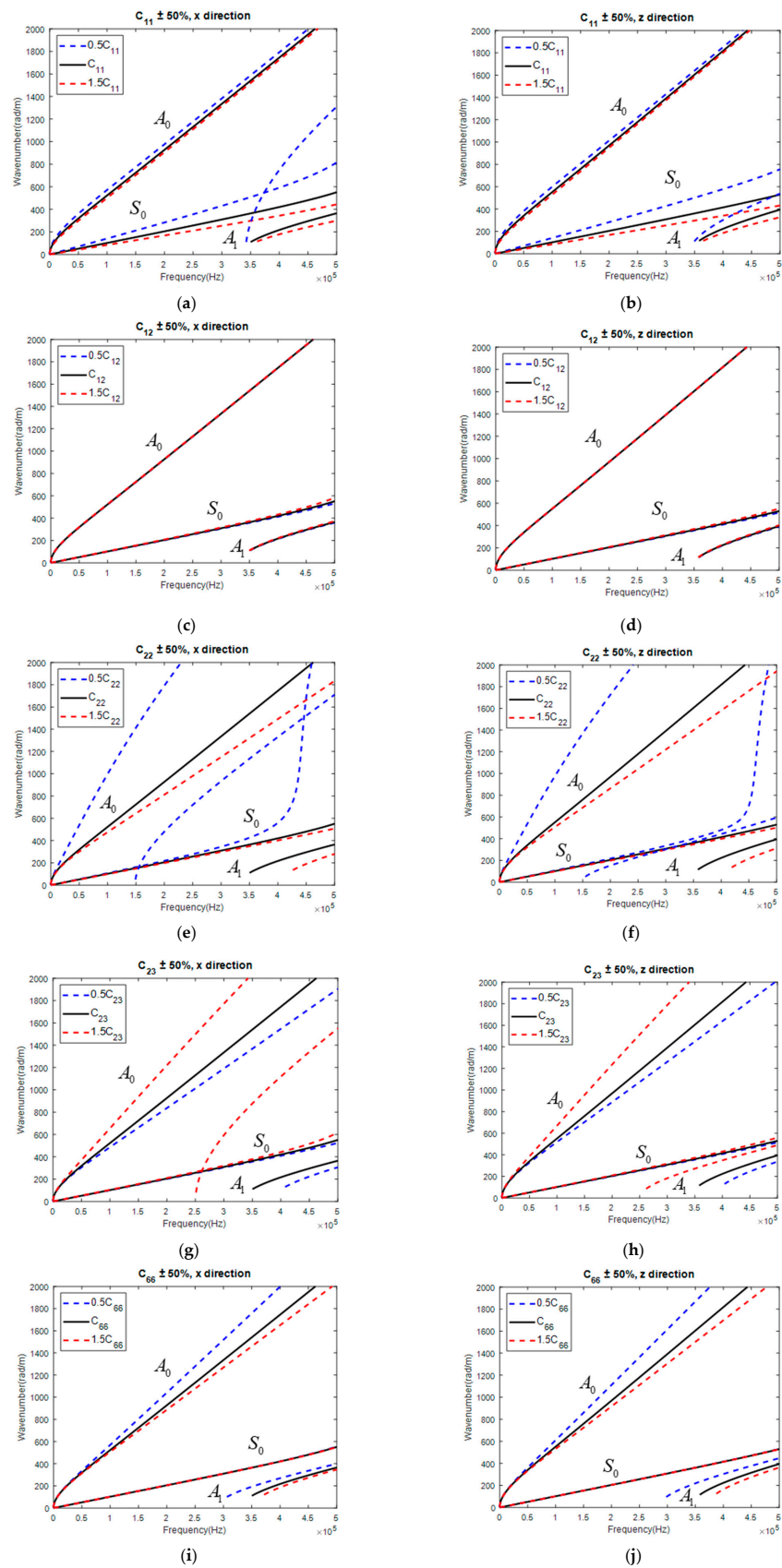


Figure 7. Influence of parameter on GW dispersion curve in CP: C_{11} on GW along (a) x and (b) z direction; C_{12} on GW along (c) x and (d) z direction; C_{22} on GW along (e) x and (f) z direction; C_{23} on GW along (g) x and (h) z direction; C_{66} on GW along (i) x and (j) z direction.

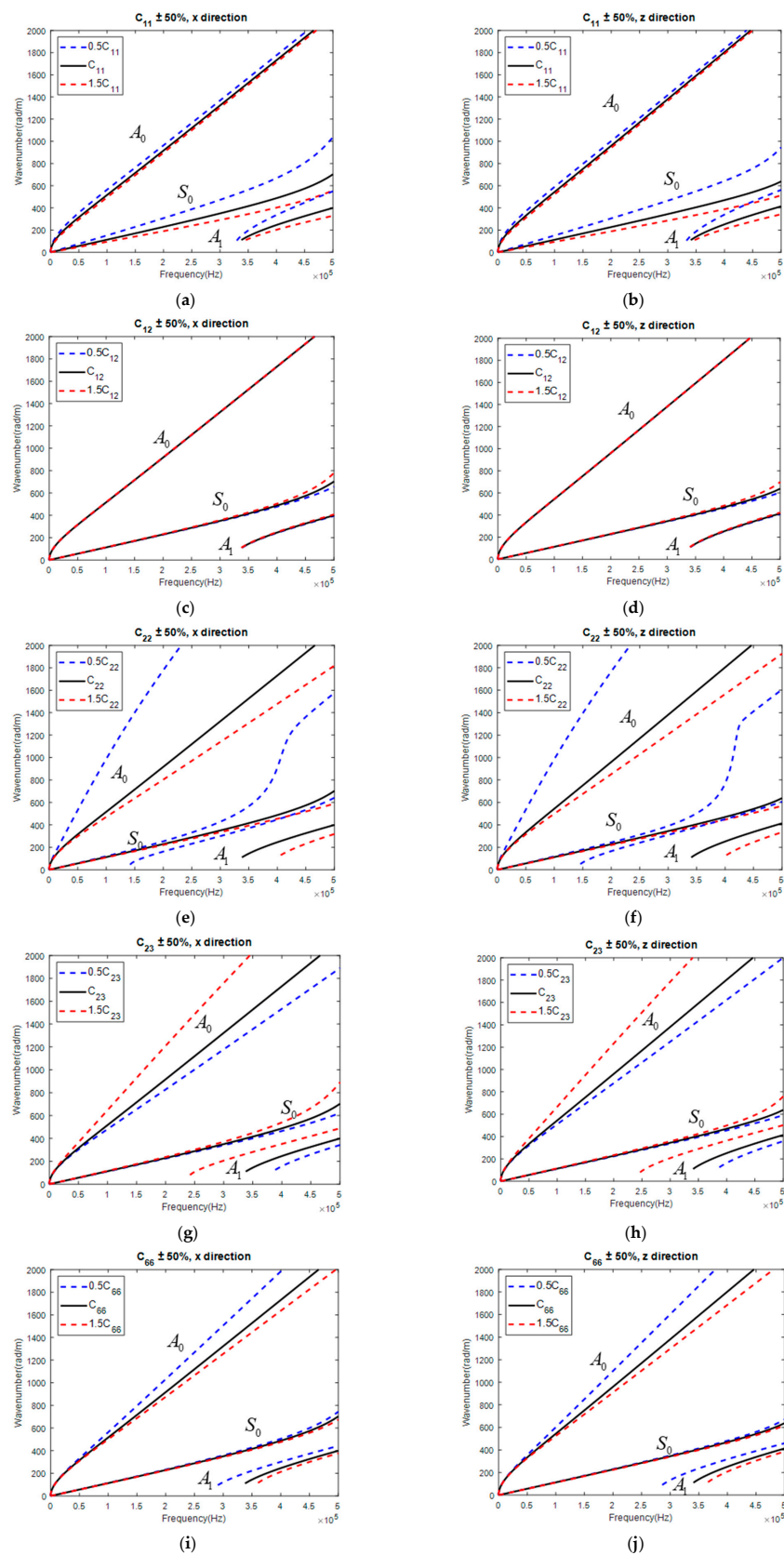


Figure 8. Influence of parameter on GW dispersion curve in QI: C_{11} on GW along (a) x and (b) z direction; C_{12} on GW along (c) x and (d) z direction; C_{22} on GW along (e) x and (f) z direction; C_{23} on GW along (g) x and (h) z direction; C_{66} on GW along (i) x and (j) z direction.

3.2. Reconstruction of Stiffness Matrix of CFRP with GW-Based GA

With the proposed GW-based GA, the reconstructed values of the stiffness matrix with different image resolutions (251×251 , 501×501 , 1001×1001 , and 2001×2001) and the maximum relative deviation in percentage defined below are listed in Table 5,

$$\delta_{ij}^k = \left| \frac{C_{ij}^k - \bar{C}_{ij}^k}{\bar{C}_{ij}^k} \times 100 \right| \quad (12)$$

where $k = 1, 2$, and 3 denote UD, CP, and QI, respectively, and \bar{C}_{ij}^k denotes the mean value of C_{ij}^k . The mean values of the maximum deviation in percentage are 27.46%, 12.40%, 17.35%, and 11.71% for image resolutions 251×251 , 501×501 , 1001×1001 , and 2001×2001 , respectively. Hence, the accuracy of the parameter reconstruction is well guaranteed at the image resolution of 501×501 , which is adopted for further analysis. Note that the calculation time before convergence is largely dependent on the random initial values and has an average time of around 20 min.

Table 5. Reconstructed stiffness matrix and maximum deviation percentage.

	Ply Stacking	Resolution	C_{11}	C_{12}	C_{22}	C_{23}	C_{66}
Value (GPa)	UD	251×251	121.10	2.08	9.33	3.67	4.23
		501×501	125.42	3.43	10.28	4.83	4.03
		1001×1001	129.79	2.87	8.94	3.22	4.13
		2001×2001	110.50	6.13	9.96	4.56	4.23
	CP	251×251	129.86	5.41	8.54	2.06	3.16
		501×501	128.70	4.69	9.57	3.67	3.55
		1001×1001	129.18	6.05	9.96	3.56	3.26
		2001×2001	126.78	5.73	11.54	4.94	3.16
	QI	251×251	125.42	2.63	11.30	3.89	3.06
		501×501	126.58	3.90	10.75	3.22	3.06
		1001×1001	128.63	2.63	9.33	3.67	4.22
		2001×2001	127.95	4.22	12.32	4.83	3.06
Maximum deviation (%)		251×251	3.50	60.38	16.21	35.76	21.44
		501×501	1.42	17.05	7.80	23.63	13.63
		1001×1001	2.93	21.82	14.24	38.66	20.93
		2001×2001	2.67	26.11	9.79	40.75	15.69

It is concluded from the reconstruction result with the image resolution of 501×501 that

- (1) The maximum deviation percentage of C_{11} is only 1.42%, which indicates that C_{11} reconstructed from the GW-based GA is highly accurate and robust.
- (2) C_{12} exerts negligible influence on the GW dispersion curves along both the x and z directions for CFRPs with the investigated three stacking sequences. Thus, a large maximum deviation of up to 17.5% should be expected.
- (3) The maximum deviation percentage of C_{22} is only 7.80%, which indicates that C_{22} reconstructed from the GW-based GA is highly accurate and robust. The mean value of the three reconstructed values of C_{22} with CFRPs of three different stacking sequences is calculated as 10.20 GPa, which is extremely close to the value of 10.28 GPa derived with tensile loading and longitudinal wave. As illustrated in Figure 6f, C_{22} exerts a significant influence on the GW dispersion curve normal to the fiber direction in unidirectional CFRP. Thus, the reconstructed value of C_{22} can be highly trusted.
- (4) C_{23} shows a maximum deviation of 23.63%. The reconstructed values from CP and QI are smaller than that from UD, which may be partially attributed to the lower sensitivity of a GW in CP and QI to C_{23} than that in UD.

- (5) C_{66} shows a maximum deviation of 13.63%. As C_{66} exerts an influence on a GW along the fiber direction (see Figure 6i) in UD and along both directions in CP (see Figure 7i,j) and QI (see Figure 8i,j), the derived result should be trusted.

Based on the reconstructed parameters, the dispersion curves were calculated and superposed with the experimentally obtained GW frequency and wave number contour, as displayed in Figure 9. The magnitude of acquired GW significantly varied among modes, frequencies, and laminates with specific stacking sequences. E.g., the S_0 mode along the fiber direction of UD was hardly visible (see Figure 9a), higher modes along the x direction were clearly acquired in CP and QI, and both A_0 and S_0 modes were acquired only around the frequency range [100 kHz, 250 kHz]. Despite partially missing information and the existence of measurement noise, all the contours were well matched with the GW dispersions curves, which proved the correctness of the adopted GA.

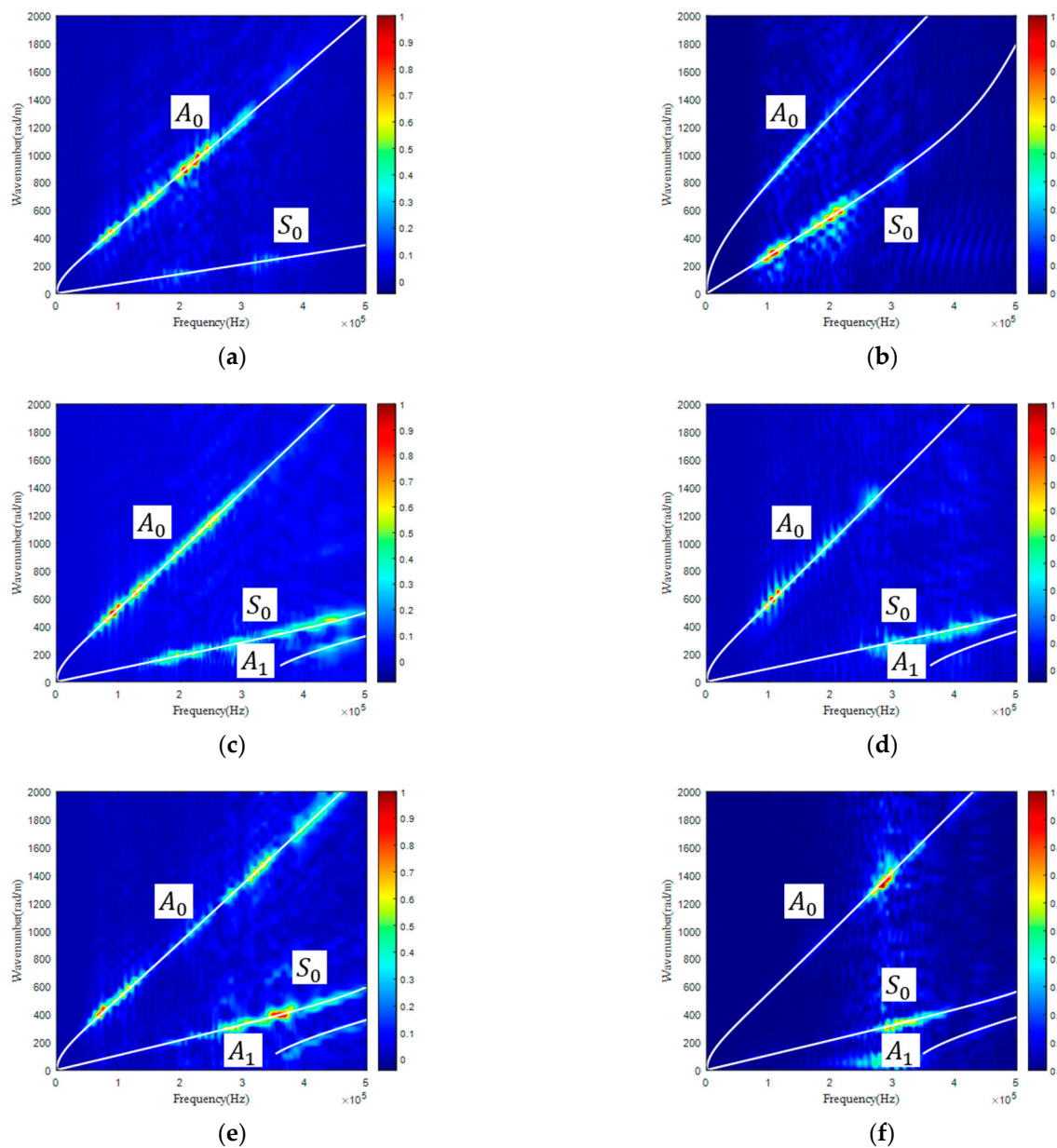


Figure 9. Experimentally obtained frequency and wave number contour superposed with the GW dispersion curve calculated with the reconstructed stiffness matrix: UD along (a) x direction and (b) z direction; CP along (c) x direction and (d) z direction; QI along (e) x direction and (f) z direction.

As C_{11} , C_{12} , and C_{66} mainly influence the GW along the fiber direction in UD, and C_{22} and C_{23} jointly decide the GW normal to the fiber direction, the parameter reconstruction for UD can be decoupled into two groups. By contrast, for CP and QI, all five parameters are coupled together to jointly determine the GW propagation along either direction. Thus, it is assumed that the parameters reconstructed from UD may be more accurate than those from other samples. In addition, the tensile loading and the longitudinal wave test are performed on UD to derive another set of parameters. Considering the mentioned two aspects, the parameters reconstructed from the GW in UD are used as a benchmark to be further compared with the obtained parameters from both tensile loading and longitudinal wave, with the deviation percentage listed in Table 6. It is concluded that

- (1) The deviation percentage of C_{11} reaches 17.80%, which indicates that the derived C_{11} from tensile loading is slightly smaller than the value from GW testing. Considering the GW-based GA obtains three values of C_{11} with only a maximum deviation of 1.42%, the tensile loading may not accurately reconstruct the value of C_{11} , possibly attributed to the incorrect cutting of the sample for tensile loading, which is further discussed in Section 3.3.1.
- (2) The deviation percentage of C_{12} reaches 61.79%, which can be attributed to the insensitiveness of GW on the change of C_{12} . This implies that more GW modes at a wider frequency range should be considered to accurately reconstruct the value of C_{12} .
- (3) The deviation percentage of C_{22} reaches 14.98%, indicating a good match. The one from the longitudinal wave actually measures the stiffness along the thickness direction, while the one from the GW combines the stiffness from both the transverse and thickness directions. This implies that the assumption of transverse isotropy is approximated and satisfied.
- (4) The deviation percentage of C_{23} reaches 10.82%, indicating a good match.
- (5) The deviation percentage of C_{66} reaches 0.53%, indicating an almost exact match.

Table 6. Deviation percentage of the measured stiffness matrix with the image resolution 501×501 .

Value	C_{11}	C_{12}	C_{22}	C_{23}	C_{66}
(%)	17.80	61.79	14.98	10.82	0.53

In conclusion, excluding C_{12} , which exerts a negligible influence on GW dispersion, an average deviation of 11.03% for the four remaining parameters in UD is achieved between the GW-based GA and the technique combining static tensile loading and longitudinal wave testing. To achieve an accurate reconstruction of C_{12} , more GW modes in a wider frequency band should be involved, as discussed in Section 3.3.2.

3.3. Further Refinement of Stiffness Matrix

3.3.1. Refinement of C_{11}

The reconstructed values of C_{11} are close to each other among the CFRPs with three stacking sequences while different from the value measured with the tensile loading test. Thus, an ultrasound C-scan of UD used for tensile loading was performed with the ultrasonic microscope (PVA TePla[®] SAM 401) to obtain raw imaging, which was further filtered with a threshold level of 113 for the measurement of fiber orientation with respect to the long edge of the sample, as displayed in Figure 10. An average angle of 9.67° was obtained with three measurements. To validate the influence of the incorrect cutting on the material parameter, a finite element modeling was performed with the material parameter listed in the second line of Table 5. After a rotation of material orientation of 9.67° , the calculated $E_{/1}$ along the long edge was 102.3 GPa, close to the calculated E_1 with only a slight deviation of 2.78 GPa, or a percentage of 2.72%. Hence, it was proved that the incorrect cutting of the sample for tensile loading resulted in a large deviation of E_1 , which dominantly determined the value of C_{11} . Also, this implies that the GW-based GA

reconstructed the value of C_{11} with only a deviation percentage of around 2.72% to the tensile loading-based standard method.

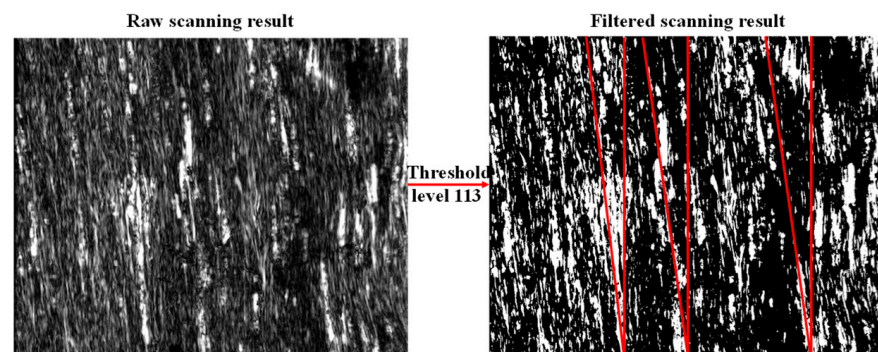


Figure 10. Ultrasound C-scan imaging of UD.

3.3.2. Refinement of C_{12}

As C_{12} is almost insensitive to the GW within the frequency range [0, 500 kHz] along both the x and z directions of CFRPs with three different stacking sequences, more GW modes within a broader frequency range [0, 1000 kHz] along the fiber direction in UD were investigated. The thickness was set at 2.05 mm, and material parameters were set according to the second line of Table 5, except that C_{12} was taken at 5.549 GPa. Keeping other parameters unchanged and C_{12} changed by 50%, the obtained GW dispersion curve is shown in Figure 11a. It was shown that the S_0 mode showed a moderate sensitivity to C_{12} . Thus, a time domain finite element analysis was performed with Abaqus/Explicit. Element CPE4R of size 0.15 mm was meshed, and a 3-cycle sinusoidal tone burst with a central frequency of 650 kHz was excited to acquire the response at 467 consecutive points at an interval of 0.15 mm. Following the same signal processing method with a 2-D FFT, C_{12} was set as the only variable in the GA. The final reconstructed value C_{12} was 5.333 GPa, which was with a deviation of 0.216 GPa, or a percentage of 3.9%, to the value calculated with tensile loading and longitudinal wave. Thus, it is expected that with multiple modes of GW in a wide frequency band, all the parameters in the stiffness matrix can be accurately characterized.

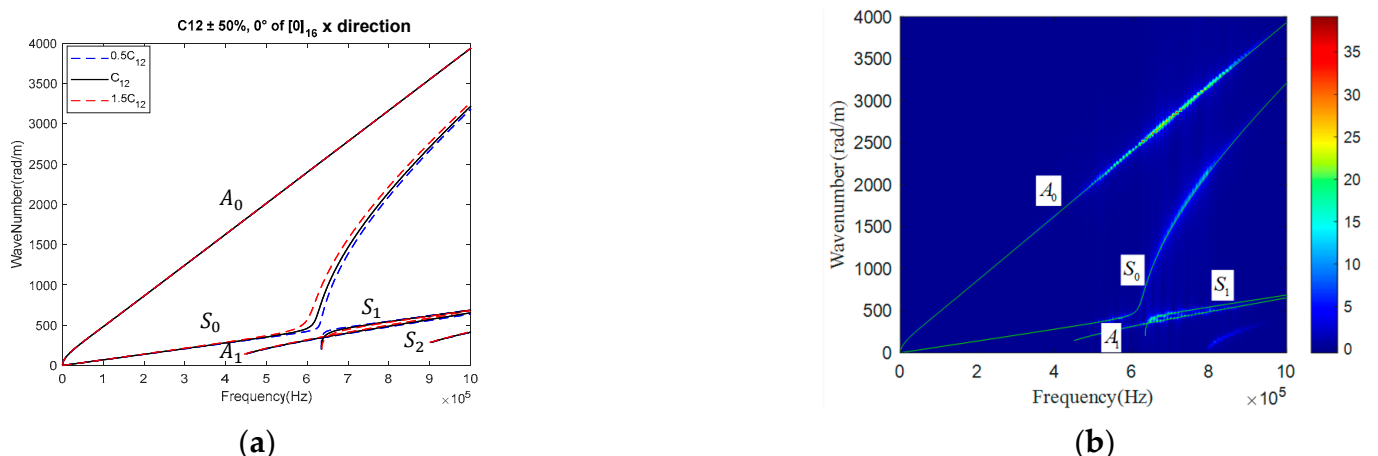


Figure 11. (a) Dispersion curve of GW along the fiber direction in UD, and (b) contour of frequency-wave number spectrogram superposed with the dispersion curve of GW based on the reconstructed C_{12} .

4. Conclusions

Multiple testing methods were performed, including GW, static tensile loading, and normally incident longitudinal waves, to reconstruct the five independent parameters in the stiffness matrix of CFRPs with unidirectional ($[0/16]_s$), cross-ply ($[0/90]_{4s}$), and

quasi-isotropic ($[0/90/0/90/45/-45/45/-45]_s$) stacking sequences. Compared with the destructive tensile loading-based technique, the proposed GW-based GA realized an automatic and nondestructive reconstruction of the stiffness matrix. For the four independent parameters in each ply of the laminate, excluding C_{12} , an average value of the maximum deviation of 11.62% was achieved among the CFRP with three different stacking sequences, and an average deviation of 11.03% for UD was achieved for the parameters measured based on different methods. Toward a further refinement of parameter characterization, the incorrect cutting of UD was compensated to reach a relative deviation of 2.72% for E_1 between a GW-based GA and destructive tensile loading. Also, with a finite element simulation that involved GW in a wider frequency range, it was proved that C_{12} can also be reconstructed with a relative deviation of 3.9%. Future work will explore the excitation and acquisition of GWs experimentally up to a wider frequency range in order to realize the simultaneous and more accurate reconstruction of a stiffness matrix. In addition, a GA usually takes around 20 min to reconstruct the parameters, which is far from the realization of real-time parameter reconstruction. Hence, the improvement of reconstruction efficiency will be focused on. Finally, an extension of the proposed technique to various materials will also be investigated in the near future.

Author Contributions: Conceptualization by M.L. and F.C.; investigation by Y.Z.; formal analysis by Y.Z. and L.L.; writing, review, and editing performed by all authors; and funding acquisition by M.L. All authors have read and agreed to the published version of the manuscript.

Funding: This research was funded by the National Natural Science Foundation of China, grant number 52105142, the Shenzhen Stable Support Grant, grant number GXWD20201230155427003-20200731161831019, and the Guangdong Basic and Applied Basic Research Foundation, grant number 2019A1515110704.

Institutional Review Board Statement: Not applicable.

Informed Consent Statement: Not applicable.

Data Availability Statement: Not applicable.

Conflicts of Interest: The authors declare no conflict of interest.

Nomenclature

CFRP	carbon fiber reinforced polymer
GA	genetic algorithm
GW	guided wave
SAFE	semi-analytical finite element method
2D-FFT	two-dimensional Fourier transform
OF	objective function
σ_i	stress
ε_i	strain
C_{ij}	elastic constants
E_i	Young's modulus
ν_{ij}	Poisson's ratio
G_{ij}	shear modulus
N_i	loading force
A	cross-sectional area of tensile sample
d	the measured thickness of tensile sample
M_{cal}	theoretically calculated images
M_{exp}	experimental images
UD	unidirectional laminate $[0]_{16}$
CP	cross-ply laminate $[0/90]_{4s}$
QI	quasi-isotropic laminate $[0/90/0/90/45/-45/45/-45]_s$

References

1. Elsheikh, A.H.; Panchal, H.; Shanmugan, S.; Muthuramalingam, T.; El-Kassas, A.M.; Ramesh, B. Recent Progresses in Wood-Plastic Composites: Pre-Processing Treatments, Manufacturing Techniques, Recyclability and Eco-Friendly Assessment. *Clean. Eng. Technol.* **2022**, *8*, 100450. [[CrossRef](#)]
2. Elsheikh, A. Bistable Morphing Composites for Energy-Harvesting Applications. *Polymers* **2022**, *14*, 1893. [[CrossRef](#)] [[PubMed](#)]
3. Abd Elaziz, M.; Elsheikh, A.H.; Oliva, D.; Abualigah, L.; Lu, S.; Ewees, A.A. Advanced Metaheuristic Techniques for Mechanical Design Problems: Review. *Arch. Comput. Methods Eng.* **2022**, *29*, 695–716. [[CrossRef](#)]
4. Bulut, M. Mechanical Characterization of Basalt/Epoxy Composite Laminates Containing Graphene Nanopellets. *Compos. Part B Eng.* **2017**, *122*, 71–78. [[CrossRef](#)]
5. Padture, N.P. Environmental Degradation of High-Temperature Protective Coatings for Ceramic-Matrix Composites in Gas-Turbine Engines. *npj Mater. Degrad.* **2019**, *3*, 11. [[CrossRef](#)]
6. Wang, X.; Gu, Y.; Chen, Y.; Ullah, Z.; Pan, Q.; Zhao, Y. A New Technology for Steel Pipeline Damage Detecting without Removing Cladding. *Measurement* **2020**, *159*, 107700. [[CrossRef](#)]
7. Ogierman, W. Inverse Identification of Elastic Properties of Constituents of Discontinuously Reinforced Composites. *Materials* **2018**, *11*, 2332. [[CrossRef](#)]
8. ASTM D7291/D7291M-15; Standard Test Method for Through-Thickness “Flatwise” Tensile Strength and Elastic Modulus of a Fiber-Reinforced Polymer Matrix Composite Material. ASTM International: West Conshohocken, PA, USA, 2022.
9. Deng, L.; Lei, L.; Lai, S.; Liao, L.; Zhou, Z. Experimental Study on the Axial Tensile Properties of FRP Grid-Reinforced ECC Composites. *Materials* **2021**, *14*, 3936. [[CrossRef](#)]
10. Kê, T.S. Development of the Torsion Pendulum and Early Research on Grain Boundary Relaxation and the Cold-Work Internal Friction Peak. *J. Alloys Compd.* **1994**, *211*, 7–15. [[CrossRef](#)]
11. Renault, A.; Jaouen, L.; Sgard, F. Characterization of Elastic Parameters of Acoustical Porous Materials from Beam Bending Vibrations. *J. Sound Vib.* **2011**, *330*, 1950–1963. [[CrossRef](#)]
12. Paolino, D.S.; Geng, H.; Scattina, A.; Tridello, A.; Cavatorta, M.P.; Belingardi, G. Damaged Composite Laminates: Assessment of Residual Young’s Modulus through the Impulse Excitation Technique. *Compos. Part B Eng.* **2017**, *128*, 76–82. [[CrossRef](#)]
13. Xie, M.; Li, F. A Modified Piezoelectric Ultrasonic Composite Oscillator Technique for Simultaneous Measurement of Elastic Moduli and Internal Frictions at Varied Temperature. *Rev. Sci. Instrum.* **2020**, *91*, 015110. [[CrossRef](#)] [[PubMed](#)]
14. Park, S.H.; Liu, P.; Yi, K.; Choi, G.; Jhang, K.Y.; Sohn, H. Mechanical Properties Estimation of Additively Manufactured Metal Components Using Femtosecond Laser Ultrasonics and Laser Polishing. *Int. J. Mach. Tools Manuf.* **2021**, *166*, 103745. [[CrossRef](#)]
15. Wong, V.-K.; Hu, Y.; Tham, Z.W.; Chen, Y.F.; Liu, M.; Lim, K.E.; Park, S.J.; Cui, F.; Zhang, L. Measurement of Elastic Constant Matrix of Carbon Fiber Composites With an Ultrasonic 2D-Array Transducer. *IEEE Sens. J.* **2022**, *22*, 5562–5570. [[CrossRef](#)]
16. Cao, H.; Guo, S.; He, Z.; Xie, Y.; Zhang, T.; Feng, W. In Situ Elastic Constant Determination of Unidirectional CFRP Composites via Backwall Reflected Multi-Mode Ultrasonic Bulk Waves Using a Linear Array Probe. *Compos. Part B Eng.* **2022**, *238*, 109953. [[CrossRef](#)]
17. Chen, J.; Bai, X.; Yang, K.; Ju, B.F. Simultaneously Measuring Thickness, Density, Velocity and Attenuation of Thin Layers Using $V(z, t)$ Data from Time-Resolved Acoustic Microscopy. *Ultrasonics* **2015**, *56*, 505–511. [[CrossRef](#)]
18. Lasn, K.; Echtermeyer, A.T.; Klauson, A.; Chati, F.; Décultot, D. Comparison of Laminate Stiffness as Measured by Three Experimental Methods. *Polym. Test.* **2015**, *44*, 143–152. [[CrossRef](#)]
19. Castaings, M.; Hosten, B.; Kundu, T. Inversion of Ultrasonic, Plane-Wave Transmission Data in Composite Plates to Infer Viscoelastic Material Properties. *NDT E Int.* **2000**, *33*, 377–392. [[CrossRef](#)]
20. Liu, M.; Wang, K.; Lissenden, C.J.; Wang, Q.; Zhang, Q.; Long, R.; Su, Z.; Cui, F. Characterizing Hypervelocity Impact (HVI)-Induced Pitting Damage Using Active Guided Ultrasonic Waves: From Linear to Nonlinear. *Materials* **2017**, *10*, 547. [[CrossRef](#)]
21. Yu, X.; Fan, Z.; Castaings, M.; Biateau, C. Feature Guided Wave Inspection of Bond Line Defects between a Stiffener and a Composite Plate. *NDT E Int.* **2017**, *89*, 44–55. [[CrossRef](#)]
22. Vishnuvardhan, J.; Krishnamurthy, C.V.; Balasubramaniam, K. Genetic Algorithm Based Reconstruction of the Elastic Moduli of Orthotropic Plates Using an Ultrasonic Guided Wave Single-Transmitter-Multiple-Receiver SHM Array. *Smart Mater. Struct.* **2007**, *16*, 1639–1650. [[CrossRef](#)]
23. Zhao, J.; Qiu, J.; Ji, H. Reconstruction of the Nine Stiffness Coefficients of Composites Using a Laser Generation Based Imaging Method. *Compos. Sci. Technol.* **2016**, *126*, 27–34. [[CrossRef](#)]
24. Glushkov, E.; Glushkova, N.; Eremin, A. Efficient Mathematical Representations for Computing the Forced Wave Dynamics of Anisotropic Laminated Composites. *CEAS Aeronaut. J.* **2013**, *4*, 11–19. [[CrossRef](#)]
25. Foiret, J.; Minonzio, J.-G.; Chappard, C.; Talmant, M.; Laugier, P. Combined Estimation of Thickness and Velocities Using Ultrasound Guided Waves: A Pioneering Study on in Vitro Cortical Bone Samples. *IEEE Trans. Ultrason. Ferroelectr. Freq. Control* **2014**, *61*, 1478–1488. [[CrossRef](#)] [[PubMed](#)]
26. Eremin, A.A.; Glushkov, E.V.; Glushkova, N.V.; Lammering, R. Evaluation of Effective Elastic Properties of Layered Composite Fiber-Reinforced Plastic Plates by Piezoelectrically Induced Guided Waves and Laser Doppler Vibrometry. *Compos. Struct.* **2015**, *125*, 449–458. [[CrossRef](#)]
27. Golub, M.V.; Doroshenko, O.V.; Arsenov, M.A.; Eremin, A.A.; Gu, Y.; Bareiko, I.A. Improved Unsupervised Learning Method for Material-Properties Identification Based on Mode Separation of Ultrasonic Guided Waves. *Computation* **2022**, *10*, 93. [[CrossRef](#)]

28. Okumura, S.; Nguyen, V.-H.; Taki, H.; Haïat, G.; Naili, S.; Sato, T. Rapid High-Resolution Wavenumber Extraction from Ultrasonic Guided Waves Using Adaptive Array Signal Processing. *Appl. Sci.* **2018**, *8*, 652. [[CrossRef](#)]
29. Yan, L.; Cunfu, H.; Guorong, S.; Bin, W.; Chung, C.-H.; Lee, Y.-C. Elastic Properties Inversion of an Isotropic Plate by Hybrid Particle Swarm-Based-Simulated Annealing Optimization Technique from Leaky Lamb Wave Measurements Using Acoustic Microscopy. *J. Nondestruct. Eval.* **2014**, *33*, 651–662. [[CrossRef](#)]
30. Hu, Y.; Cui, F.; Li, F.; Tu, X.; Zeng, L. Sparse Wavenumber Analysis of Guided Wave Based on Hybrid Lasso Regression in Composite Laminates. *Struct. Heal. Monit.* **2022**, *21*, 1367–1378. [[CrossRef](#)]
31. Bochud, N.; Laurent, J.; Bruno, F.; Royer, D.; Prada, C. Towards Real-Time Assessment of Anisotropic Plate Properties Using Elastic Guided Waves. *J. Acoust. Soc. Am.* **2018**, *143*, 1138–1147. [[CrossRef](#)]
32. Liu, M.; Li, L.; Zhang, Y.; Chen, G.; Cui, F. Dispersion of Guided Waves in Complex Waveguides: A Hybrid Modeling Technique Combining Gauss-Lobatto-Legendre Node Collation and Semi-Analytical Finite Element Method. *Int. J. Appl. Mech.* **2022**. [[CrossRef](#)]